Growth of Ga_2O_3 Nanowires via Cu-As-Ga Ternary Phase Diagram

Hang Wang [1,2,†], **Ying Wang** [2,3,†], **Shuyan Gong** [2], **Xinyuan Zhou** [2], **Zaixing Yang** [4], **Jun Yang** [1,5,*], **Ning Han** [2,3,*] and **Yunfa Chen** [2,3,*]

1 School of Metallurgical Engineering, Xi'an University of Architecture and Technology, Xi'an 710055, China; 13572151480@163.com
2 State Key Laboratory of Multiphase Complex Systems, Institute of Process Engineering, Chinese Academy of Sciences, Beijing 100190, China; wangying@ipe.ac.cn (Y.W.); shuyangong@ipe.ac.cn (S.G.); zhouxinyuan14@mails.ucas.ac.cn (X.Z.)
3 Center for Excellence in Regional Atmospheric Environment, Institute of Urban Environment, Chinese Academy of Sciences, Xiamen 361021, China
4 Center of Nanoelectronics and School of Microelectronics, Shandong University, Jinan 250100, China; zaixyang@sdu.edu.cn
5 Metallurgical Engineering and Technology Research Center of Shaanxi Province, Xi'an 710055, China
* Correspondence: yj-yangjun@xauat.edu.cn (J.Y.); nhan@ipe.ac.cn (N.H.); chenyf@ipe.ac.cn (Y.C.); Tel.: +86-13152420820 (J.Y.); +86-010-6255-8356 (N.H.)
† These authors contributed equally to this work.

Abstract: Currently, it is challenging to develop new catalysts for semiconductor nanowires (NWs) growth in a complementary-metal-oxide-semiconductor (CMOS) compatible manner via a vapor-liquid-solid (VLS) mechanism. In this study, chemically synthesized Cu_2O nano cubes are adopted as the catalyst for single crystalline β-Ga_2O_3 NWs growth in chemical vapor deposition. The growth temperature is optimized to be 750 to 800 °C. The NW diameter is controlled by tuning the sizes of Cu_2O cubes in the 20 to 100 nm range with a bandgap of ~4.85 eV as measured by ultraviolet-visible absorption spectroscopy. More importantly, the catalyst tip is found to be Cu_5As_2, which is distinguished from those Au-catalyzed Au-Ga alloys. After a comprehensive phase diagram investigation, the β-Ga_2O_3 NWs are proposed to be grown by the ternary phase of Cu-As-Ga diffusing Ga into the growth frontier of the NW, where Ga react with residual oxygen to form the NWs. Afterward, Ga diminishes after growth since Ga would be the smallest component in the ternary alloy. All these results show the importance of the catalyst choice for CMOS compatible NW growth and also the potency of the ternary phase catalyst growth mode in other semiconductor NWs synthesis.

Keywords: Ga_2O_3 nanowires; Cu_2O cubes; Cu_5As_2; Cu-As-Ga ternary phase diagram; chemical vapor deposition

1. Introduction

In recent years, Ga_2O_3 nanowires (NWs) with a wide bandage of ~4.9 eV have attracted greater attention because of the unique structural, electronic, mechanical, and optical properties, such as having a Debye length comparable to the small size and tuned band gap based on size restriction, which is applicable to various electronic and optical nano-devices [1–8]. Previously, numerous methods were employed to grow Ga_2O_3 NWs including pulsed laser deposition (PLD), molecular beam epitaxy (MBE), and thermal evaporation, via the well-established vapor-liquid-solid (VLS) mechanism [7,9–18]. Typically, Au nanoparticles are widely adopted as the catalyst for the NWs

growth, which behaves as a precursor pyrolysis catalyst and a nucleation center in numerous NWs growth including Ga_2O_3, GaAs, Si, and other semiconductors [17,19–24]. However, Au might diffuse into the silicon substrate, forming foreign impurities and deep level dopants and, thus, degenerate the electronic properties [25,26]. Therefore, it is necessary to adopt substitute metal catalysts for the complementary-metal-oxide-semiconductor (CMOS) compatibility [21,27,28].

In past research studies, to solve this problem, self-catalyzed growth methods and CMOS compatible metal catalyst induced growth technologies that have been developed for the semiconductor NWs growth [15,16,28]. However, complicated substrate treatment would be desired in order to obtain a diameter uniform NW growth because NW diameters would vary greatly if there is no foreign catalyst in the self-catalyzed growth [15]. In addition, many scholars have tried new catalysts such as Ag and Co materials to obtain Ga_2O_3 NWs [29,30]. However, thermally annealing the metal films, which are physically deposited by thermal and/or e-beam evaporation that mainly form the catalyst particles. In the meantime, Cu is a good CMOS compatible metal, and has been adopted for the Si NW growth [31–34]. However, whether Cu or potential cuprous oxide plays the role in the catalytic growth process is deliberated. For instance, Vincent et al. fabricated Si NWs using copper-based catalysts and finding the original seed layer that is absolutely oxidized to Cu_2O at the optimum oxygen pressure by comparing different oxygen pressures for producing straight NWs [27]. Thus, progress in designing more appropriate Ga_2O_3 NWs agreeing with CMOS requires a clear understanding of the nature of the Cu catalyst and a controllable tunability of the catalyst.

In this study, chemically-synthesized Cu_2O nanoparticles are adopted as catalysts for β-Ga_2O_3 NWs growth on Si/SiO_2 substrates by the chemical vapor deposition method using GaAs powders as the source. The optimum growth temperature is 750–800 °C and the NW diameter is successfully tuned by regulating different Cu_2O particle sizes in the range of 20 to 100 nm. The synthesized β-Ga_2O_3 NWs are single crystalline with a bandgap of ~4.85 eV (256 nm) as obtained by ultraviolet-visible absorption spectroscopy. The catalyst tip is found to be Cu_5As_2 alloy, without any Ga component within the resolution of the energy dispersive spectroscopy. This is different from the Au-Ga alloy catalyst in Au-catalyzed growth, which is further studied by analyzing the Cu-As-Ga ternary phase diagram to explore the growth mechanism.

2. Materials and Methods

In this study, the Ga_2O_3 NWs are synthesized in a solid-source chemical vapor deposition (SSCVD) system utilizing GaAs powders as the source material (0.5 g, 99.999% purity), and chemically synthesized Cu_2O as the catalyst. Cu_2O was fabricated with a controlled cube morphology and diameter between 25 to 177 nm, as shown in the supporting information (Figure S1). Then, Cu_2O nano cube catalysts were dispersed on the surface of the <100>-oriented Si/SiO_2 (50 nm thick thermally grown oxide) substrates. A horizontal tube furnace was used as the reactor with the GaAs source placed in the middle of the heating zone and the catalyst in the downstream (3 cm away from the source zone) of the zone with a tilt angle of about 20°. Prior to the growth of NWs, the substrates were cleaned with ultrasonic bath in deionized water, ultrapure water, and ethanol for 5 min, and dried by the nitrogen blow. In the process of growth, the reacting system was evacuated to about 10 mtorr and purged by Ar (99.999% pure) gas at 100 standard cubic centimeter per min (sccm) for 10 min. The substrate and the source were heated to the preset growth temperature (700 °C to 900 °C) synchronously. The growth time was 90 min and a constant flow rate of Ar gas at 100 sccm was maintained in the quartz tube during the growth process. Lastly, the system was cooled down to room temperature and the white Ga_2O_3 NWs were harvested.

The surface morphologies of the grown Ga_2O_3 NWs were examined clearly with a scanning electron microscope (SEM, JEOL JSM-6700F, Japan, 15 kV, 10 mA). High-resolution transmission electron microscopy (HRTEM) images and corresponding energy dispersive spectroscopy (EDS) of NWs were obtained on a JEOL JEM-2100F microscope with an accelerating voltage of 200 kV. The crystallinity of grown Ga_2O_3 NWs was investigated by employing an X-ray diffractometer with

Cu Kα radiation (1.5406 Å) operated at 40 kV and 40 mA in the diffraction angle (2θ) range from 20° to 70°. The ultraviolet-visible absorption spectrum was recorded on a LAMBDA 750 spectrophotometer (Perkin Elmer, Waltham, MA, USA) at room temperature.

3. Results and Discussion

In order to study the effect of temperature on the growth of Ga_2O_3 NWs catalyzed by Cu_2O, 25 nm Cu_2O cubes were adopted as catalysts to find the optimal growth conditions. Figure 1a–e show the SEM images of Ga_2O_3 NWs grown at various temperatures and insets are corresponding cross-sectional SEM images illustrating the length of the NWs. To further quantify the influence of the temperature on the NW growth rate, corresponding NW length and growth rate are plotted in Figure 1f. Through comparative observations, we can see NWs grow sparsely at 700 °C with a low growth rate. This can be interpreted by limited gallium source vaporized and deposited because of low temperature, which leads to insufficient super-saturation of the catalyst droplets on the downstream substrates. From growth speed of NWs and corresponding illustrations, we conclude that 750 to 800 °C is the promising temperature for NW growth, which possesses a good NW uniformity and straightness. Many twists and bends occur in NWs at 850 °C in Figure 1d and NWs become shorter and more disordered as the temperature keeps rising until 900 °C, which is shown in Figure 1e. Ultimately, original morphology disappears when replaced by the nano-cone structure when the temperature reaches 900 °C. This is because the super-saturation of droplets decreases with the increase of growth temperature, which slows down the nucleation and reduces the growth rate, according to the Gibbs Thomson model in Equation (1) [28,35].

$$\text{v} = \left(\frac{\sqrt{b}\Delta\mu}{kT}\right)^2 = \left(\frac{\sqrt{b}\Delta\mu_0}{kT} - \frac{\sqrt{b}4\Omega a_{vs}}{kTd}\right)^2 \tag{1}$$

where k is Boltzmann's constant, b is a kinetic coefficient of crystallization, $\Delta\mu_0$ is the super-saturation in the planar limit, Ω is the atomic volume of the growth species, a_{vs} is the average surface energy density of the NW surface facets, and T is the temperature. The given explanation for the phenomenon could be that the growth rate is inversely proportional to growth temperature affecting the length of NWs (L = vt). Furthermore, the role of source gas pressure, though usually not considered a pivotal factor, is actually crucial in determining NWs synthesis [36]. However, the density of the NWs is not perfect. It would be decided by the Cu_2O catalyst nanoparticles used since they are grown by the VLS mechanism, which might also be tuned by the catalyst density. A low growth rate might be due to the new ternary phase diagram and also the low growth temperature.
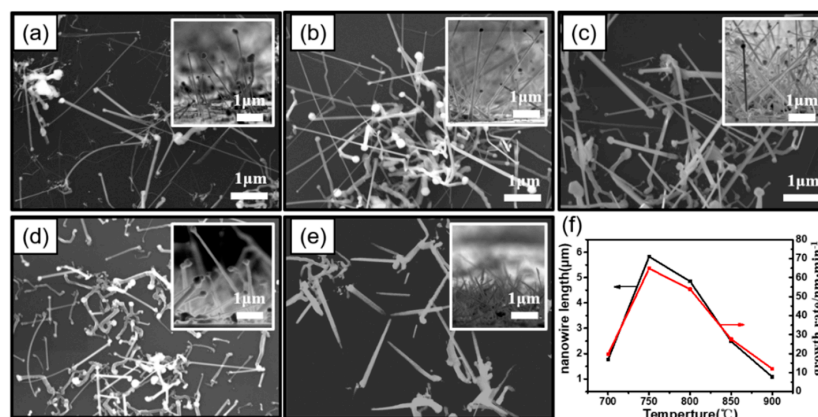

Figure 1. SEM surface images of Ga_2O_3 NWs grown at various temperatures. (**a**) 700 °C, (**b**) 750 °C, (**c**) 800 °C, (**d**) 850 °C, (**e**) 900 °C, and (**f**) relationship between the length and growth rate of NWs and growth temperature. Inset of (**a**–**e**) are magnified cross-sectional SEM images illustrating the length of the NWs. From NWs growth speed, 750 to 800 °C is a promising temperature.

Five sizes of Cu_2O particles were synthesized by adjusting NaOH concentration (supporting information, Table S1) [37]. Based on the TEM images, the mean lengths of Cu_2O cube edges and the NW average diameters can be determined by the statistics of 50 individual catalyst cubes and NWs synthesized by different sizes of Cu_2O as a catalyst (supporting information, Table S2). Figure 2 shows the relationship between the Ga_2O_3 NW diameter and the Cu_2O cube size obtained at the optimum growth temperature of 750 °C. It is observed that the diameters of NWs strongly depend upon the size of the Cu_2O catalyst within 20 to 100 nm. When the size of the catalyst is over 100 nm, a huge diversity emerges between the diameter of the catalyst and synthesized NWs. Specifically, a large fluctuation in catalyst size led to the growth of NWs with low uniformity, while a relatively good size uniformity of the catalyst resulted in the production of highly uniform NWs, which was proven by statistics of standard deviations of NWs diameter presented in the red cross. This phenomenon can be explained by the critical diameter of the VLS mechanism because a high supersaturation is necessary in the VLS mechanism, as shown in Equation (1), which is inversely related with a catalyst diameter. In fact, a larger size means smaller supersaturation (Gibbs Thomson effect) for effective NWs growth by VLS, which can be exhibited by Equation (1). This can also be inferred from Figure 1b that thin NWs can grow longer than thicker ones. In addition, when the diameter is larger than its critical diameter, NWs would possibly grow via the vapor solid (VS) mechanism. For example, Choi et al. found that the growth of NWs follows the VS mechanism when the catalyst size is larger than 65 nm catalyzed by sputtered thin films [38–42].
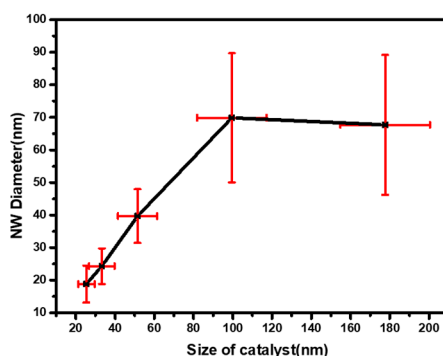
Figure 2. Relationship between the NW diameter grown at 750 °C and average size of the catalyst.

For the further structural and chemical characterization, the Ga_2O_3 NWs were then investigated using TEM, as shown in Figure 3a, where a typical Ga_2O_3 NW is observed with a smooth surface and a hemispherical tip. Inset is corresponding EDS mapping of the NW, from which we can see Ga and O are uniformly distributed in the NWs body, and As and Cu are concentrated in the catalytic head. The typical elemental composition and the typical spectra of the tip and body is analyzed by EDS, which are illustrated in Figure 3b,c. More specifically, the element line scan also clearly shows the distribution of the four elements in Figure 3d. These results evidently show that the obtained NWs are Ga_2O_3 grown via the VLS mechanism with the possible catalytic tips of the Cu-As alloy. It should also be emphasized that no As-related signal is obtained in the NW body within the detection limit of EDS performed in this study. This would be attributed to the fact that Ga_2O_3 has a far lower Gibbs free energy (approximately −998.3 kJ/mol) than GaAs (−67.8 kJ/mol) [43]. Therefore, it is more preferentially grown from the thermal dynamics point of view. In the meantime, GaAs decomposes at a higher temperature than 650 °C and, thus, As would be hard to bind with Ga. In addition, the introduction of As requires a high-energy ion implantation method. The experimental conditions are extremely harsh and it is impossible to introduce As doping by the conventional CVD method [44,45]. In addition, it is noted that GaAs particles are adopted as the source instead of metallic gallium, since GaAs particles can evaporate Ga to give the precursor in a relatively low temperature of 750 to 800 °C. On the contrary, if metallic Ga is used, it will form a liquid metal and a very high temperature (e.g., 1000 °C, [46]), which is needed to evaporate enough Ga precursors.
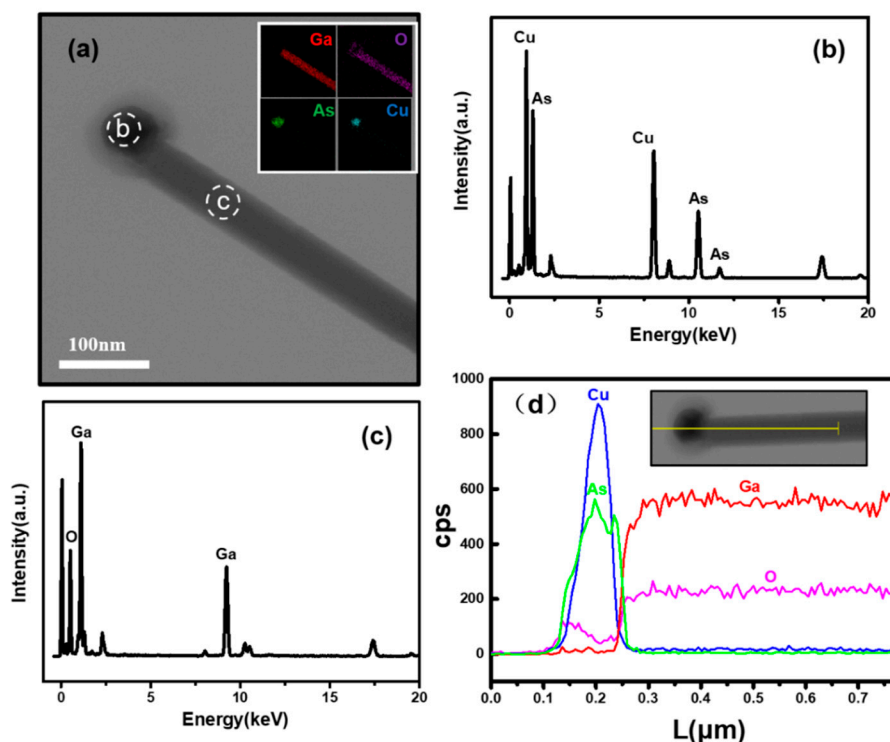
Figure 3. Elemental distribution of the NWs. (**a**) TEM image of a typical Ga_2O_3 NW and inset is EDS mapping of the NW, (**b**) EDS spectrum of the tip, (**c**) EDS spectrum of the NW body, and (**d**) EDS line scan along this NW. The curves indicate the distribution of Cu, As, Ga, and O elements along the axial direction of the NW. It can be clearly seen that the wire is Ga_2O_3 and the catalyst tip is the Cu-As alloy.

To investigate the crystal structure of the NWs, XRD patterns are obtained, as shown in Figure 4a, where a structure and phase purity of β-Ga_2O_3 is confirmed with the diffraction pattern in good agreement with the monoclinic β-Ga_2O_3 structure. Figure 4b shows the HRTEM and corresponding fast Fourier transformation (FFT) images of the NWs, which indicates a single crystalline structure. Lattice fringes of $(1\bar{1}\bar{1})$, $(\bar{2}\bar{1}1)$, and $(\bar{3}02)$ planes are marked in the images, which correspond well with the β-Ga_2O_3 phase. In the meantime, the growth direction of the NW can be indexed to be $[1\bar{1}\bar{1}]$ by the FFT in the inset. On the other hand, though similar fringes of (111), $(\bar{1}02)$, and $(\bar{2}\bar{1}1)$ planes are indexed in Figure 4c, which verifies the β-Ga_2O_3 phase, the growth orientation is different from $[\bar{1}02]$, as indexed by the selected area electron diffraction (SAED) pattern. Non-uniform growth directions under one growth condition are also reported in the literature. For example, $[111]$, $[001]$, $[\bar{1}30]$ and so on [13,47–49], which might be a result of the thermodynamics favoring the lowest surface energy. The HRTEM images of the top region is shown in Figure 4d and a spacing of about 0.289 nm is measured, which corresponds to the distance between (010) planes of the Cu_5As_2 phase (PDF No. 00-013-0581). In addition, the FFT of the catalyst tip in the inset image also show similar (010) and (121) planes, which infers the possible catalytic tip of the Cu-As alloy. We analyzed the crystal structure of several other obtained catalyst tips and found that their crystal plane spacings were also about 0.289 nm, as shown in Figure S2a–c. By consulting the alloys formed by Cu and As, we found that, among the possible phases, including Cu_5As_2, Cu_3As, Cu_6As, Cu_9As, $CuAs_2$ and Cu_2As, the 0.289 nm crystal plane spacing only exists in orthorhombic Cu_5As_2. This is also in agreement with the atomic ratio of Cu: As of 2.3 (69.43%:30.57%) in the EDS data in Figure S2d.
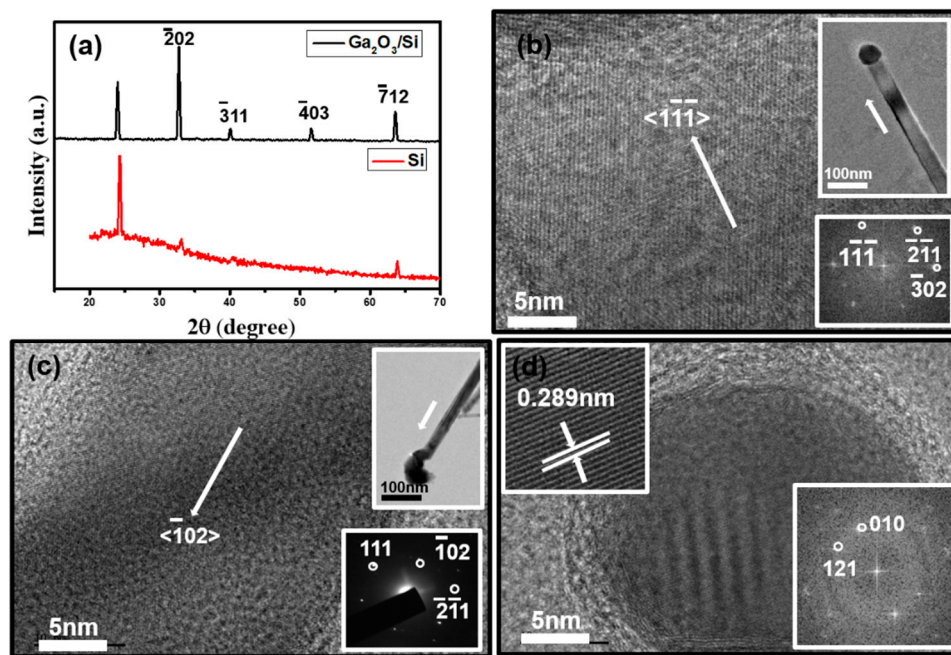
Figure 4. Crystal structure characterizations of the NWs. (**a**) XRD patterns of the NWs and the Si/SiO$_2$ substrate, (**b**) HRTEM image of NW grown along the <1$\bar{1}\bar{1}$> direction, according to FFT images in the inset for one of a representative Ga$_2$O$_3$ NWs, (**c**) another NW grown along the <$\bar{1}$02> direction as identified by the SAED pattern in the inset, and (**d**) HRTEM image and FFT (inset) of the Cu$_5$As$_2$ alloy tips.

To explore the bandgap information of the Ga$_2$O$_3$ NWs, ultraviolet-visible absorption spectrum is obtained, which is shown in Figure 5. Tauc's equation was normally adopted, and the bandgap is calculated from the plot of $(\alpha h\nu)^2$ vs hν. It clearly displays that the band gaps edge lies at approximately 4.85 eV (256 nm) of the β-Ga$_2$O$_3$ NWs grown at 750 °C, according to extrapolated line cuts of the abscissa axis. This is in good agreement with research studies [50].
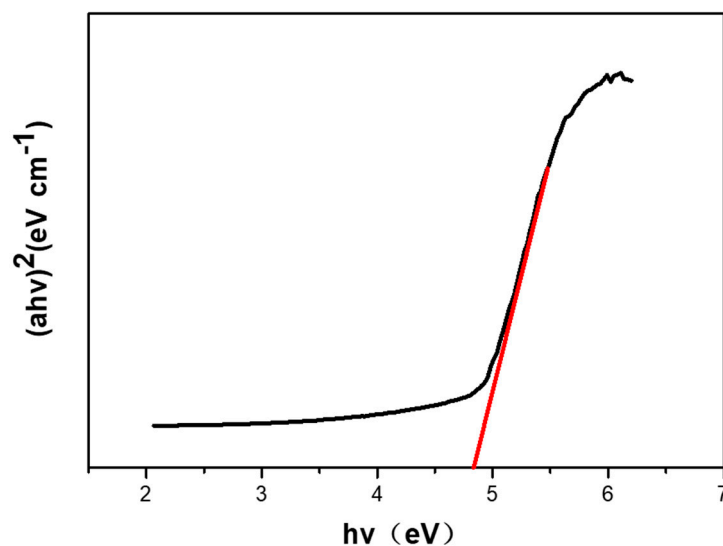
Figure 5. Ultraviolet-visible absorption spectrum of the β-Ga$_2$O$_3$ NWs.

Lastly, we analyzed the formation mechanism of β-Ga$_2$O$_3$ NWs catalyzed by Cu$_2$O, as schematically shown in Figure 6. During the experiment, we quickly increased the furnace temperature to 750 °C in 20 min, when GaAs starts to evaporate to provide the Ga and As precursors

to the growth substrate. In addition, the Cu_2O cubic nanoparticles start to decompose into Cu droplets and then react with Ga and As to form $Cu_xAs_yGa_z$ ternary alloy, according to the VLS mechanism. The saturation of the alloy droplets continues to increase, and then Ga choose the most favorable direction to start reacting with residual oxygen to initiate NW growth and generate an interface with a clear boundary as the NW growth front. In a stable growth environment of 90 min, more Ga and As volatilize and transfer to be absorbed on the catalyst drop by maintaining a concentration gradient of the component of the liquid alloy, which results in a small super-saturation leading the incorporation of new mater at the drop-NW interface to further extend the NWs [51–53].
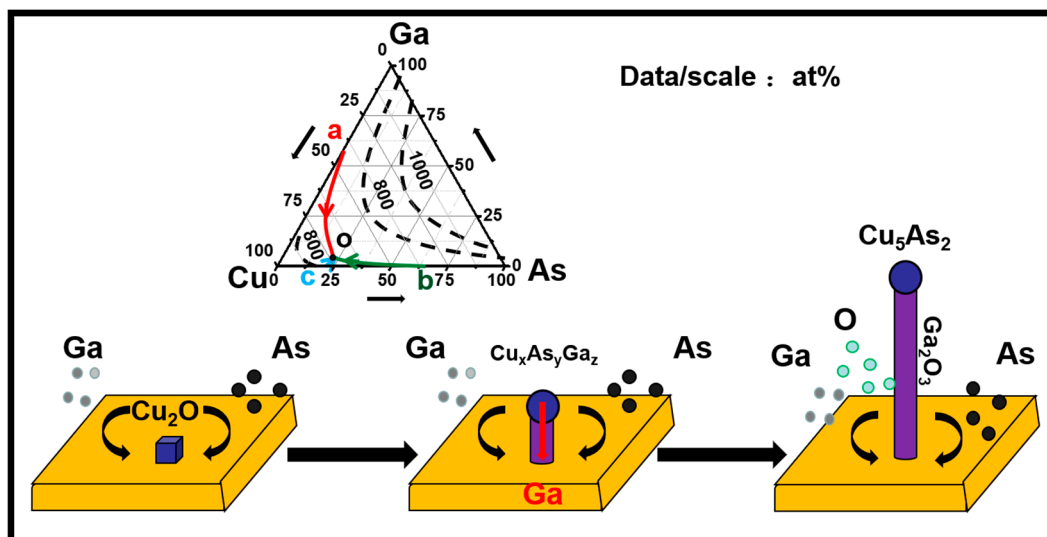
Figure 6. Schematic illustration of the β-Ga_2O_3 NWs growth process. The Cu_2O nano cube catalysts first decomposes to form Cu droplets, which then absorb Ga and As precursors to form a $Cu_xAs_yGa_z$ catalyst alloy. The Ga precursors then diffuse through the alloy and then react with residual oxygen to form the NWs. Above the picture is the Cu-As-Ga ternary alloy phase diagram. The red, green, and blue curves represent the alloy wire lines, and the dotted lines are the temperature curves. The eutectic point can be clearly seen in the diagram to form the Cu_5As_2 alloy phase.

In order to explain the cause of formation of the catalyst head and the mechanism of phase transformation, liquidus projection of the Cu–As–Ga system is shown in Figure 6 [54–56]. Three vertices of a triangle represent three pure components of Cu, As, Ga, respectively, and three sides of the equilateral triangle, which indicate the alloys formed by the corresponding two elements. The red, green, and blue lines are Ga-Cu, Cu_5As_2, and Cu_3As binary alloy equilibrium lines. From the phase diagram, ternary eutectic point temperature is under 700 °C and, at this ternary eutectic point 'o', the contents of three components are Cu: 73%, As: 25%, and Ga: 2%, which is in good agreement with our experiment results of Cu: 69.43% and As: 30.57% (atomic ratio). The incorporation and deposition of Ga would follow the red line in the phase diagram, and the content of Ga is decreasing from 'a' to 'o.' Lastly, at the end of the growth process, Ga species in the catalyst alloy droplets were consumed in the formation of Ga_2O_3 NWs, while the remaining Cu and all the As species were solidified to the Cu_5As_2 phase. To conclude, continuous Ga atoms flow into the $Cu_xAs_yGa_z$ sophisticated phase and increase the super-saturation of the alloy. Therefore, it pushes NWs interfacial layer growth, which proceeds until the temperature is naturally cooled to room temperature. The reaction can be described as Equations (2)–(4) [19].

$$Ga(l) + O_2(g) \rightarrow Ga_2O_3(s) \tag{2}$$

$$Ga(l) + Ga_2O_3(s) \rightarrow Ga_2O(g) \tag{3}$$

$$Ga_2O(g) + O_2(g) \rightarrow Ga_2O_3(s) \tag{4}$$

Therefore, VLS growth of Ga_2O_3 NWs is actually dominated by the phase equilibrium of the Cu-As-Ga alloy catalyst. In addition, all those results show the importance and potency of the catalyst choice for semiconductor NWs growth through a ternary phase diagram.

4. Conclusions

Single crystalline β-Ga_2O_3 NWs are grown by the solid-source chemical vapor deposition method at 750 to 800 °C based on chemically synthesized Cu_2O catalytic nanoparticles scattered on the Si/SiO$_2$ substrate. The NWs diameter is dependent on the Cu_2O nanotube size in the range of 20 to 100 nm. The NWs growth orientation is varied to be a mixture of [$1\overline{1}\overline{1}$] and [$\overline{1}02$] and the NWs bandgap is ~4.85 eV. The catalyst tip after growth is found to be orthorhombic Cu_5As_2, which infers a VLS growth mode of the NWs where Ga is diffused from Cu-As-Ga ternary alloy to the growth front and then is reacted with the residual oxygen. All these results indicate that the successful synthesis of a large-bandgap Ga_2O_3 NWs material based on chemically assisted incubation of CMOS compatible catalysts, which is also promising for other semiconductor NWs synthesis.

Supplementary Materials: TEM and diameter distribution of Cu_2O nanoparticle catalyst and corresponding NW. This material is available free of charge via the Internet at http://www.mdpi.com/2073-4352/9/3/155/s1. Figure S1: The broad views of several different sizes Cu_2O cubes synthesized by chemical methods. Table S1: Synthesis conditions of Cu_2O using ascorbic acid as a reductive agent. Table S2: Catalyst size, NW diameter, and corresponding standard deviation. Figure S2a–c: HRTEM of catalyst heads of different Ga_2O_3 NWs and d is the TEM image and elemental atomic ratio of the tip.

Author Contributions: The paper was written through contributions of all authors. All authors have given approval to the final version of the paper. Conceptualization, H.W. Data curation, H.W., Y.W., and X.Z. Formal analysis, H.W. Investigation, H.W. and Y.W. Methodology, H.W., Y.W., and S.G. Project administration, N.H. and Y.C. Resources, H.W., Y.W., and Z.Y. Software, S.G. and X.Z. Validation, J.Y. Visualization, J.Y. Writing—original draft, H.W. and Y.W. Writing—review & editing, J.Y. and N.H.

Conflicts of Interest: The authors declare no conflict of interest.

References

1. Yang, H.; Shuanglin, Y.; Zhongli, W.; Qiang, W.; Chengying, S.; Xu, Z.; Bai, X.D.; Chengcun, T.; Changzhi, G. Preparation and electrical properties of ultrafine Ga_2O_3 nanowires. *J. Phys. Chem. B* **2006**, *110*, 796–800.

2. Higashiwaki, M.; Jessen, G.H. Guest Editorial: The dawn of gallium oxide microelectronics. *Appl. Phys. Lett.* **2018**, *112*, 060401. [CrossRef]

3. Huang, Y.; Wang, Z.L.; Wang, Q.; Gu, C.Z.; Tang, C.C.; Bando, Y.; Golberg, D. Quasi-Aligned Ga_2O_3 Nanowires Grown on Brass Wire Meshes and Their Electrical and Field-Emission Properties. *J. Phys. Chem. C* **2009**, *113*, 1980–1983. [CrossRef]

4. Yan, R.X.; Gargas, D.; Yang, P.D. Nanowire photonics. *Nat. Photonics* **2009**, *3*, 569–576. [CrossRef]

5. Zhang, Y.Y.; Wu, J.; Aagesen, M.; Liu, H.Y. III-V nanowires and nanowire optoelectronic devices. *J. Phys. D-Appl. Phys.* **2015**, *48*, 463001. [CrossRef]

6. Xing, C.K.L.; Zhenzhong, Z.; Chunrui, W.; Binghui, L.; Haifeng, Z.; Dongxu, Z.; Dezhen, S. A Self-Powered Solar-Blind Photodetector with Fast Response Based on Au/β-Ga_2O_3 Nanowires Array Film Schottky Junction. *Acs Appl. Mater. Interfaces* **2016**, *8*, 4185–4191.

7. Ali, H.; Zhang, Y.Y.; Tang, J.; Peng, K.; Sun, S.B.; Sun, Y.; Song, F.L.; Falak, A.; Wu, S.Y.; Qian, C.J.; et al. High-Responsivity Photodetection by a Self-Catalyzed Phase-Pure p-GaAs Nanowire. *Small* **2018**, *14*, 1704429. [CrossRef]

8. Bae, J.; Kim, H.W.; Kang, I.H.; Yang, G.; Kim, J. High breakdown voltage quasi-two-dimensional beta-Ga_2O_3 field-effect transistors with a boron nitride field plate. *Appl. Phys. Lett.* **2018**, *112*, 122102. [CrossRef]

9. Bae, H.J.; Yoo, T.H.; Yoon, Y.; Lee, I.G.; Kim, J.P.; Cho, B.J.; Hwang, W.S. High-Aspect Ratio beta-Ga_2O_3 Nanorods via Hydrothermal Synthesis. *Nanomaterials* **2018**, *8*, 594. [CrossRef]

10. Choi, Y.C.; Kim, W.S.; Park, Y.S.; Lee, S.M.; Bae, D.J.; Lee, Y.H.; Park, G.S.; Choi, W.B.; Lee, N.S.; Kim, J.M. Catalytic growth of beta-Ga_2O_3 nanowires by arc discharge. *Adv. Mater.* **2000**, *12*, 746–750. [CrossRef]

11. Dai, Z.R.; Pan, Z.W.; Wang, Z.L. Gallium oxide nanoribbons and nanosheets. *J. Phys. Chem. B* **2002**, *106*, 902–904. [CrossRef]

12. Hu, J.Q.; Li, Q.; Meng, X.M.; Lee, C.S.; Lee, S.T. Synthesis of beta-Ga_2O_3 nanowires by laser ablation. *J. Phys. Chem. B* **2002**, *106*, 9536–9539. [CrossRef]

13. Li, J.Y.; Qiao, Z.Y.; Chen, X.L.; Chen, L.; Cao, Y.G.; He, M.; Li, H.; Cao, Z.M.; Zhang, Z. Synthesis of beta-Ga_2O_3 nanorods. *J. Alloy. Compd.* **2000**, *306*, 300–302. [CrossRef]

14. Zhang, H.Z.; Kong, Y.C.; Wang, Y.Z.; Du, X.; Bai, Z.G.; Wang, J.J.; Yu, D.P.; Ding, Y.; Hang, Q.L.; Feng, S.Q. Ga_2O_3 nanowires prepared by physical evaporation. *Sol. State Commun.* **1999**, *109*, 677–682. [CrossRef]

15. Kumar, S.; Tessarek, C.; Sarau, G.; Christiansen, S.; Singh, R. Self-Catalytic Growth of β-Ga_2O_3 Nanostructures by Chemical Vapor Deposition. *Adv. Eng. Mater.* **2015**, *17*, 709–715. [CrossRef]

16. Sinha, G.; Datta, A.; Panda, S.K.; Chavan, P.G.; More, M.A.; Joag, D.S.; Patra, A. Self-catalytic growth and field-emission properties of Ga_2O_3 nanowires. *J. Phys. D-Appl. Phys.* **2009**, *42*, 185409. [CrossRef]

17. Ning, H.; Fengyun, W.; Zaixing, Y.; Senpo, Y.; Guofa, D.; Hao, L.; Ming, F.; Takfu, H.; Ho, J.C. Low-temperature growth of highly crystalline β-Ga_2O_3 nanowires by solid-source chemical vapor deposition. *Nanoscale Res. Lett.* **2014**, *9*, 347.

18. Chang, K.W.; Wu, J.J. Low-temperature growth well-aligned beta-Ga_2O_3 nanowires from a single-source organometallic precursor. *Adv. Mater.* **2004**, *16*, 545–549. [CrossRef]

19. Chun, H.J.; Choi, Y.S. Controlled Structure of Gallium Oxide Nanowires. *Mrs Proc.* **2003**, *789*, 9042–9046. [CrossRef]

20. Han, N.; Wang, F.; Hou, J.J.; Yip, S.P.; Lin, H.; Fang, M.; Xiu, F.; Shi, X.; Hung, T.F.; Ho, J.C. Manipulated Growth of GaAs Nanowires: Controllable Crystal Quality and Growth Orientations via a Supersaturation-Controlled Engineering Process. *Cryst. Growth Des.* **2012**, *12*, 6243–6249. [CrossRef]

21. Ning, H.; Hou, J.J.; Fengyun, W.; Senpo, Y.; Yu-Ting, Y.; Zai-Xing, Y.; Guofa, D.; Takfu, H.; Yu-Lun, C.; Ho, J.C. GaAs nanowires: From manipulation of defect formation to controllable electronic transport properties. *Acs Nano* **2013**, *7*, 9138–9146.

22. Ning, H.; Zai-Xing, Y.; Fengyun, W.; Guofa, D.; Senpo, Y.; Xiaoguang, L.; Tak Fu, H.; Yunfa, C.; Ho, J.C. High-Performance GaAs Nanowire Solar Cells for Flexible and Transparent Photovoltaics. *Acs Appl. Mater. Interfaces* **2015**, *7*, 20454–20459.

23. Wang, Y.; Hou, L.; Qin, X.; Ma, S.; Zhang, B.; Gou, H.; Gao, F. Fabrication of Single-Crystalline β-Ga_2O_3 Nanowires and Zigzag-Shaped Nanostructures. *J. Phys. Chem. C* **2007**, *111*, 17506–17511. [CrossRef]

24. Zhou, W.; Ying, W.; Zhou, X.; Yang, Z.; Yin, Y.; Jie, Z.; Ning, H.; Ho, J.C.; Chen, Y. Controlled Growth of Heterostructured Ga/GaAs Nanowires with Sharp Schottky Barrier. *Cryst. Growth Des.* **2018**, *18*, 4438–4444.

25. Du, Y.J.A.; Sakong, S.; Kratzer, P. As vacancies, Ga antisites, and Au impurities in zinc blende and wurtzite GaAs nanowire segments from first principles. *Phys. Rev. B* **2013**, *87*, 075308. [CrossRef]

26. Morante, J.R.; Carceller, J.E.; Herms, A.; Cartujo, P.; Barbolla, J. Dpendence of the electron cross-section for the acceptor gold level in silion on the gold to donor ratio. *Appl. Phys. Lett.* **1982**, *41*, 656–658. [CrossRef]

27. Renard, V.T.; Michael, J.; Patrice, G.; Peter, C.; Denis, R.; Amal, C.; Vincent, J. Catalyst preparation for CMOS-compatible silicon nanowire synthesis. *Nat. Nanotechnol.* **2009**, *4*, 654–657. [CrossRef]

28. Zhang, Y.; Sanchez, A.M.; Sun, Y.; Wu, J.; Aagesen, M.; Huo, S.; Kim, D.; Jurczak, P.; Xu, X.; Liu, H. Influence of Droplet Size on the Growth of Self-Catalyzed Ternary GaAsP Nanowires. *Nano Lett.* **2016**, *16*, 1237–1243. [CrossRef]

29. Nguyen, T.D.; Kim, E.T.; Dao, K.A. Ag nanoparticle catalyst based on Ga_2O_3/GaAs semiconductor nanowire growth by VLS method. *J. Mater. Sci. Mater. Electron.* **2015**, *26*, 8747–8752. [CrossRef]

30. Wang, H.; Lan, Y.; Zhang, J.; Crimp, M.A.; Ren, Z. Growth mechanism and elemental distribution of beta-Ga_2O_3 crystalline nanowires synthesized by cobalt-assisted chemical vapor deposition. *J. Nanosci. Nanotechnol.* **2012**, *12*, 3101–3107. [CrossRef]

31. Arbiol, J.; Kalache, B.; Cabarrocas, P.R.I.; Morante, J.R.; Morral, A.F.I. Influence of Cu as a catalyst on the properties of silicon nanowires synthesized by the vapour-solid-solid mechanism. *Nanotechnology* **2007**, *18*, 305606. [CrossRef]

32. Yao, Y.; Fan, S. Si nanowires synthesized with Cu catalyst. *Mater. Lett.* **2007**, *61*, 177–181. [CrossRef]

33. Kim, S.; Jung, S.; Kim, M.H.; Cho, S.; Lee, J.H.; Park, B.G. Switching and Conduction Mechanism of Cu/Si$_3$N$_4$/Si RRAM with CMOS Compatibility. In *2014 Silicon Nanoelectronics Workshop (SNW)*; IEEE: New York, NY, USA, 2014.

34. Zhu, S.Y.; Chu, H.S.; Lo, G.Q.; Kwong, D.L. CMOS-Compatible Plasmonic Bragg Reflectors Based on Cu-Dielectric-Si Structures. *IEEE Photonics Technol. Lett.* **2013**, *25*, 2115–2118. [CrossRef]

35. Ek, M.; Borg, B.M.; Johansson, J.; Dick, K.A. Diameter Limitation in Growth of III-Sb-Containing Nanowire Heterostructures. *Acs Nano* **2013**, *7*, 3668–3675. [CrossRef] [PubMed]

36. Kodambaka, S.; Tersoff, J.; Reuter, M.C.; Ross, F.M. Germanium nanowire growth below the eutectic temperature. *Science* **2007**, *316*, 729–732. [CrossRef] [PubMed]

37. Gong, S.Y.; Wu, X.F.; Zhang, J.L.; Han, N.; Chen, Y.F. Facile solution synthesis of Cu$_2$O-CuO-Cu(OH)$_2$ hierarchical nanostructures for effective catalytic ozone decomposition. *Crystengcomm* **2018**, *20*, 3096–3104. [CrossRef]

38. Mandl, B.; Keplinger, M.; Messing, M.E.; Kriegner, D.; Wallenberg, R.; Samuelson, L.; Bauer, G.; Stangl, J.; Holy, V.; Deppert, K. Self-Seeded Axio-Radial InAs-InAs1-xPx Nanowire Heterostructures beyond "Common" VLS Growth. *Nano Lett.* **2018**, *18*, 144–151. [CrossRef]

39. Dhalluin, F.; Baron, T.; Ferret, P.; Salem, B.; Gentile, P.; Harmand, J.C. Silicon nanowires: Diameter dependence of growth rate and delay in growth. *Appl. Phys. Lett.* **2010**, *96*, 133109. [CrossRef]

40. Du, W.N.; Yang, X.G.; Pan, H.Y.; Wang, X.Y.; Ji, H.M.; Luo, S.; Ji, X.H.; Wang, Z.G.; Yang, T. Two Different Growth Mechanisms for Au-Free InAsSb Nanowires Growth on Si Substrate. *Cryst. Growth Des.* **2015**, *15*, 2413–2418. [CrossRef]

41. Kashchiev, D. Dependence of the growth rate of nanowires on the nanowire diameter. *Cryst. Growth Des.* **2006**, *6*, 1154–1156. [CrossRef]

42. Choi, K.H.; Cho, K.K.; Cho, G.B.; Ahn, H.J.; Kim, K.W. The growth behavior of β-Ga$_2$O$_3$ nanowires on the basis of catalyst size. *J. Cryst. Growth* **2009**, *311*, 1195–1200. [CrossRef]

43. Speight, J. *Lange's Handbook of Chemistry*; Mc Graw-Hill: New York, NY, USA, 2005.

44. Izhnin, I.I.; Voitsekhovsky, A.V.; Korotaev, A.G.; Fitsych, O.I.; Bonchyk, A.Y.; Savytskyy, H.V.; Mynbaev, K.D.; Varavin, V.S.; Dvoretsky, S.A.; Mikhailov, N.N.; et al. Optical and electrical studies of arsenic-implanted HgCdTe films grown c with molecular beam epitaxy on GaAs and Si substrates. *Infrared Phys. Technol.* **2017**, *81*, 52–58. [CrossRef]

45. Lo, C.C.; Simmons, S.; Lo Nardo, R.; Weis, C.D.; Tyryshkin, A.M.; Meijer, J.; Rogalla, D.; Lyon, S.A.; Bokor, J.; Schenkel, T.; et al. Stark shift and field ionization of arsenic donors in Si-28-silicon-on-insulator structures. *Appl. Phys. Lett.* **2014**, *104*, 193502. [CrossRef]

46. Feng, P.; Zhang, J.Y.; Li, Q.H.; Wang, T.H. Individual beta-Ga$_2$O$_3$ nanowires as solar-blind photodetectors. *Appl. Phys. Lett.* **2006**, *88*, 153107. [CrossRef]

47. Han, W.Q.; Kohler-Redlich, P.; Ernst, F.; Ruhle, M. Growth and microstructure of Ga$_2$O$_3$ nanorods. *Sol. State Commun.* **2000**, *115*, 527–529. [CrossRef]

48. Li, J.Y.; Chen, X.L.; Qiao, Z.Y.; He, M.; Li, H. Large-scale synthesis of single-crystalline beta-Ga$_2$O$_3$ nanoribbons, nanosheets and nanowires. *J. Phys. Condens. Matter* **2001**, *13*, L937–L941. [CrossRef]

49. Liang, C.H.; Meng, G.W.; Wang, G.Z.; Wang, Y.W.; Zhang, L.D.; Zhang, S.Y. Catalytic synthesis and photoluminescence of beta-Ga$_2$O$_3$ nanowires. *Appl. Phys. Lett.* **2001**, *78*, 3202–3204. [CrossRef]

50. He, T.; Zhao, Y.K.; Zhang, X.D.; Lin, W.K.; Fu, K.; Sun, C.; Shi, F.F.; Ding, X.Y.; Yu, G.H.; Zhang, K.; et al. Solar-blind ultraviolet photodetector based on graphene/vertical Ga$_2$O$_3$ nanowire array heterojunction. *Nanophotonics* **2018**, *7*, 1557–1562. [CrossRef]

51. Chengyu, H.; Xizhang, W.; Qiang, W.; Zheng, H.; Yanwen, M.; Jijiang, F.; Yi, C. Phase-equilibrium-dominated vapor-liquid-solid growth mechanism. *J. Am. Chem. Soc.* **2010**, *132*, 4843–4847.

52. Sutter, E.; Sutter, P. Phase diagram of nanoscale alloy particles used for vapor-liquid-solid growth of semiconductor nanowires. *Nano Lett.* **2008**, *8*, 411–414. [CrossRef] [PubMed]

53. Zhang, Y.; Cai, J.; Wu, Q.; Wang, X.; Yang, L.; He, C.; Hu, Z. Phase-equilibrium-dominated vapor-liquid-solid mechanism: Further evidence. *Sci. China Mater.* **2016**, *59*, 20–27. [CrossRef]

54. Engler, N.; Leipner, H.S.; Scholz, R.F.; Schreiber, J.; Werner, P. Interaction of Copper and Sulfur with Dislocations in GaAs. In *Solid State Phenomena*; Trans Tech Publications: Zurich-Uetikon, Switzerland, 2001; Volume 78–79, pp. 331–340.

55. Hultgren, R.; Desai, P.J.; Hawkins, D.T.; Gleiser, M.; Kelley, K.K. *Selected Values of the Thermodynamic Properties of Binary Alloys*; American Society for Metals: Berkeley, CA, USA, 1973.

56. Hansen, M. *Constitution of Binary Alloys*; McGraw-Hill Book Company: New York, NY, USA, 1958.